Collective colloid diffusion under soft two-dimensional confinement

S. Panzuela,[1,*] Raúl P. Peláez,[2] and R. Delgado-Buscalioni[3,†]

[1]*Departmento de Fisica de la Materia Condensada, Universidad Autonoma de Madrid, Campus de Cantoblanco, Madrid 28949, Spain*

[2]*Universidad Autonoma de Madrid, Ciudad Universitaria de Cantoblanco, 28049 Madrid, Spain*

[3]*Departmento de Fisica de la Materia Condensada, Universidad Autonoma de Madrid, and Institute for Condensed Matter Physics, IFIMAC, Campus de Cantoblanco, Madrid 28049, Spain*

(Received 25 October 2016; published 5 January 2017)

This work presents a numerical and theoretical investigation of the collective dynamics of colloids in an unbounded solution but trapped in a harmonic potential. Under strict two-dimensional confinement (infinitely stiff trap) the collective colloidal diffusion is enhanced and diverges at zero wave number (like k^{-1}), due to the hydrodynamic propagation of the confining force across the layer. The analytic solution for the collective diffusion of colloids under a Gaussian trap of width δ still shows enhanced diffusion for large wavelengths $k\delta < 1$, while a gradual transition to normal diffusion for $k\delta > 1$. At intermediate and short wavelengths, we illustrate to what extent the hydrodynamic enhancement of diffusion is masked by the conservative forces between colloids. At very large wavelengths, the collective diffusion becomes faster than the solvent momentum transport and a transition from Stokesian dynamics to inertial dynamics takes place. Using our inertial coupling method code (resolving fluid inertia), we study this transition by performing simulations at small Schmidt number. Simulations confirm theoretical predictions for the $k \to 0$ limit [Phys. Rev. E **90**, 062314 (2014)] showing negative density-density time correlations. However, at finite k simulations show deviations from the theory.

DOI: 10.1103/PhysRevE.95.012602

I. INTRODUCTION

Interfaces usually induce the formation of colloid density gradients which significantly increases their mesoscopic ordering in layers. This effect is quite general and affects macromolecules and proteins around cells and organelle membranes. The layering effect is even stronger in charged or partially charged colloids near surfaces [1].

In other instances, colloids might be trapped in fluid-fluid interfaces and interact via capillary forces [2] and also by electrostatic forces [3]. Nanosize colloids (proteins) frequently move in planar membranes or vesicles being exposed to relatively large spatial fluctuations. These "sticking" scenarios, common in subcellular biology, are also relevant for many industrial problems involving the spreading of molecules within things as disparate as food, creams, or crude oil (e.g., asphaltenes near water interfaces) and more. Yet another area of technological applications uses ultrasound forces (acoustophoresis) to manipulate and confine micron-size colloids in layers [4–7]. A standing pressure wave with hundreds of megahertz or more creates an ultrasound potential which moves heavy colloidal particles towards two-dimensional traps formed at the node of the pressure wave (or the valleys if particles are lighter than the fluid) [6,7]. The resulting ultrasound potential is harmonic, leading to a Gaussian colloidal dispersion around the pressure node [7]. Similar harmonic traps can be obtained by laser tweezers [8]. Other forms of (non-Gaussian) traps can be prepared using electric fields (maybe leading to barometric-like density profiles).

The hydrodynamic coupling between the confining force acting on each individual colloid and their collective motion leads to surprising effects, most of them detected some years ago [9] and recently theoretically and experimentally revised [10,11]. Basically, momentum conservation implies that the confining force acting on each colloid has to propagate to the surrounding fluid. This propagation has the form of flow field which reaches quite long distances and affects the motion of distant colloids over the plane. Mathematically, the constraint can be also holonomic ($z_i = 0$ for each colloid i), and the confining force can be seen to arise from the nonzero divergence of the mobility tensor, which is related to the reduction of entropy imposed across the confining plane. In the case of a pointwise force in unbounded fluid such flow perturbation (Oseen) decays like $1/r$ and, as a consequence, the diffusion coefficient of longer and longer colloidal density fluctuations does increase without bounds. (In particular, the collective diffusion diverges like $D_c \sim 1/k$, where k is the wave number.) Somewhat paradoxically, or at least counterintuitive, is the fact that the single-particle diffusion coefficient might be completely unaware of this anomalous enhancement of the collective diffusion. In fact, the phenomenon also takes place in ideal particles (without potential interactions), where, irrespective of the confinement, the self-diffusion coefficient is just given by the Stokes-Einstein value $D_0 = k_B T/(6\pi\eta a)$ (where η is the fluid viscosity and a is the particle radius). It has to be said that such types of hydrodynamic enhancements do not only take place when the fluid is unbounded in the three directions. The presence of distant boundaries modifies the propagation (e.g., $1/r^2$ under the presence of up-and-down walls [12,13]), leading to yet-unexplained and stronger variations of this phenomena (diffusion diverging like $1/k^{1.7}$) which might also depend on the type of flow slippage near the wall.

The question we pose here is how this anomalous collective diffusion becomes *normal* as the confinement is made *softer*. There are several ways to gradually transform a perfect two-dimensional (2D) confinement into an isotropic 3D distribution and, as illustrated in Fig. 1, here we study the case where

*sergio.panzuela@uam.es

†rafael.delgado@uam.es

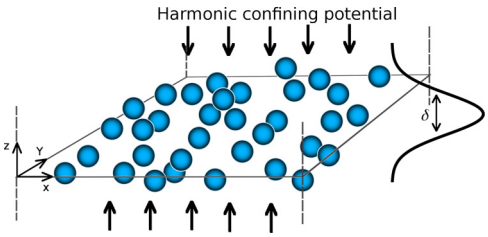

FIG. 1. Sketch of the setup of the colloidal assembly trapped in a soft Gaussian trap of width δ.

the 2D interface of colloids becomes Gaussianly blurred. In particular, we consider a suspension of colloids confined in the z direction by a parabolic potential of the form $U_e(z) = (k_s/2)(z - z_0)^2$ applied to each individual colloid. The spring constant k_s controls the width of the Gaussian distribution of colloids in the z direction,

$$\delta = \left(\frac{k_B T}{k_s}\right)^{1/2}. \tag{1}$$

This lengthscale governs the collective intermediate scattering function of colloids under harmonic confinement derived in Sec. II. Excluded volume and other potential interactions between colloids adds another lengthscale to the collective diffusion which partially masks the anomalous hydrodynamic enhancement. This masking depends on the static structure factor $S(k)$ details, and here we illustrate the case of repulsive and attractive potentials of Lennard-Jones type. Another question which intrigues us is the transition to an inertial regime taking place at very large wavelengths. If the collective diffusion scales like $D_c \propto k^{-1}$, below some small wave number k_c, then collective mass diffusion will eventually become faster than vorticity diffusion. This issue, an many others related to this problem, was studied by Dominguez *et al.* [14] showing that, for any colloidal system, the crossover should take place at macroscopic lengthscales $k_c \sim \text{mm}^{-1}$, being proportional to the inverse of the Schmidt number. Our computational method enables to artificially decrease the Schmidt number to observe the transition to the inertial regime and the appearance of damped (oscillatory) density fluctuations. Results are compared with theoretical predictions based on for the $k \to 0$ limit [14].

The manuscript is ordered as follows: In Sec. II we review the theoretical framework and present the analytical solution for the collective diffusion of ideal tracers (colloids with no potential interactions) under soft confinement. In Sec. III A we present and discuss the results for the strict confinement case, and the effects of colloidal attractive and repulsive potential interactions. In Sec. IV we validate the theoretical result for the collective diffusion of ideal tracers under soft confinement with simulations and discuss several physical scenarios where this effect could be relevant. In Sec. V we study the crossover from overdamped to nonoverdamped density fluctuations where the inertia of the solvent becomes relevant. The numerical methods used for simulations including hydrodynamic interactions (HI), performed with our graphical processors units (GPU) code FLUAM [15], are explained in Appendix B 1. Simulations without HI (independent Brownian walkers) were performed with the GROMACS package and details are also given in Appendix B 2.

II. THEORY

One of the most useful quantities to study the dynamics of colloidal density fluctuations is the intermediate collective dynamic scattering function, F_c, which can be directly measured from light-scattering experiments. In this section we derive an analytical relation for F_c defined as the time autocorrelation of the Fourier transform of the colloid density field,

$$F_c(\mathbf{k},t) = \langle \rho(\mathbf{k},t)\rho^*(\mathbf{k},t_0)\rangle, \tag{2}$$

with

$$\rho(\mathbf{k},t) = \int \rho(\mathbf{r},t)\exp(-i\mathbf{k}\cdot\mathbf{r})d\mathbf{r}, \tag{3}$$

and the microscopic density

$$\rho(\mathbf{r},t) = \sum_i \delta(\mathbf{r} - \mathbf{q}_i(t)), \tag{4}$$

as a function of the Eulerian position coordinate $\mathbf{q}_1, \ldots, \mathbf{q}_N$ of the colloidal particles at time t. Colloidal suspension normally evolve in so-called Stokes limit, where the transport of fluid momentum perturbations is much faster than the single-particle mass diffusion and thus fluid accelerations can be neglected. Albeit it has been predicted [16] that across very large wavelengths the collective, mass diffusion becomes faster than momentum transport. This crossover will be studied by numerical simulations in Sec. V. The following theoretical derivation applies strictly to the Stokes limit.

There are several ways to derive analytical expressions for the time relaxation of colloidal density fluctuations. One can combine the continuity equation for the colloidal mass and the Stokes equation for the fluid momenta, as done by Bleibel *et al.* [10].[1] Here we use another standard route (see Dhont's book [17]) which, consistently with the Stokes limit, is based on the Smoluchovsky equation for the N-particle probability distribution. The conservation of colloidal mass over any volume is formally written as $\partial_t \rho = -\nabla \cdot \mathbf{J}$, where the mass flux is assumed proportional to the density gradient $J(\mathbf{r},t) = -\int D(\mathbf{r} - \mathbf{r}',t)\nabla\rho(\mathbf{r}')d\mathbf{r}'$. Consistent with the Stokes limit, we have neglected any time-dependent memory in the nonlocal diffusion coefficient. Applying the Fourier transform to the resulting equation for ρ, and using the convolution theorem, one gets

$$\frac{\partial\rho(\mathbf{k},t)}{\partial t} = -k^2 D(\mathbf{k},t)\rho(\mathbf{k},t). \tag{5}$$

Multiplying by $\rho^*(\mathbf{k},0)$ in Eq. (5) and performing the ensemble average one gets a dynamic equation for F_c,

$$\frac{\partial F_c(\mathbf{k},t)}{\partial t} = -k^2 D(\mathbf{k},t)F_c(\mathbf{k},t), \tag{6}$$

[1] In principle, this route accesses the long-time diffusion; however, to do so it requires a linear approximation of the density field fluctuation and a mean-field approximation for the force field (which is made proportional to the density gradient to close the equation). Such an approximation precludes the observation of the distinctive features of the long-time diffusion regime.

whose solution in rotationally invariant systems (spherical colloids) is just

$$F_c(k,t) = S(k)\exp[-k^2 D_c(k,t)t], \tag{7}$$

with $S(k) = \langle \rho(k)\rho^*(k)\rangle$ being the static structure function and $D_c(\mathbf{k},t) = \frac{1}{t}\int_0^t D(\mathbf{k},t')dt'$ the collective diffusion coefficient.

To access to some microscopic expression for the collective diffusion D_c, one can use the Smoluchovsky equation for the conditional probability distribution function $P(\mathbf{q},t|\mathbf{q}_0,t_0)$ (we use the supervector notation $\mathbf{q} = \mathbf{q}_1,\ldots,\mathbf{q}_N$),

$$\frac{\partial P(\mathbf{q},t|\mathbf{q}_0,t_0)}{\partial t} = \hat{\mathcal{L}}_S P(\mathbf{q},t|\mathbf{q}_0,t_0), \tag{8}$$

where the Smoluchovsky operator $\hat{\mathcal{L}}_S$ is given by

$$\hat{\mathcal{L}}_S \square = \nabla_q \cdot \mathcal{M}(\mathbf{q})\big[\nabla_q \Phi \square + k_B T \nabla_q \square\big], \tag{9}$$

where the $\square$ symbol indicates any function of $\mathbf{q}$, $\mathcal{M}(\mathbf{q})$ is the microscopic mobility of the colloids (which in general depends on all the particles and contains hydrodynamic couplings) and $\Phi(\mathbf{q})$ is the potential of mean force, or free energy, of the colloidal assembly. The equilibrium condition guarantees that $P(\mathbf{q}) = \mathcal{Z}^{-1}\exp[-\beta\Phi(\mathbf{q})]$, with $\beta = 1/k_B T$ and the partition function given by normalization $\mathcal{Z} = \int \exp[-\beta\Phi(\mathbf{q})]dq^{3N}$. The formal solution of the Smoluchovsky equation for an assembly of colloids with prepared initial condition $\delta(\mathbf{q}-\mathbf{q}_0)$ and $\mathbf{q}_0 = \mathbf{q}(t=0)$ gives the conditional probability for the system to have a configuration $\mathbf{q}$ at time t provided it had $\mathbf{q}_0$ at t_0. Formally, it is written as $P(\mathbf{q},t|\mathbf{q}_0,t_0) = \exp[\hat{\mathcal{L}}_S(t-t_0)]\delta(\mathbf{q}-\mathbf{q}_0)$. The time correlator in Eq. (2) can be written as $\int d\mathbf{q}\rho(\mathbf{k})\exp[\hat{\mathcal{L}}_S^*(t-t_0)][\rho^*(\mathbf{k})P(\mathbf{q},t_0)]$ where $P(\mathbf{q},t_0)$ is the equilibrium distribution. Integration by parts on this expression finally leads to an expression which can be written in the form of an ensemble average at equal times,

$$F_c(\mathbf{k},t) = \int \rho^*(\mathbf{k})P(\mathbf{q},t_0)\exp[\hat{\mathcal{L}}_S^*(t-t_0)]\rho(\mathbf{k})dq^{3N}, \tag{10}$$

where $\rho(\mathbf{k}) = \sum_i \exp(-i\mathbf{k}\cdot\mathbf{q}_i)$ depends on colloid positions according to Eqs. (3) and (4). The ensemble average is notated as

$$F_c(\mathbf{k},t) = \langle \rho^*(\mathbf{k}) e^{\hat{\mathcal{L}}_S^* t}\rho(\mathbf{k})\rangle. \tag{11}$$

This expression involves the adjoint operator of $\hat{\mathcal{L}}_S$,

$$\hat{\mathcal{L}}_S^* \square = (k_B T\nabla_q - \nabla_q\Phi)\cdot\mathcal{M}(\mathbf{q})\cdot\nabla_q\square. \tag{12}$$

The short-time expansion of the exponential operator $\exp[\hat{\mathcal{L}}_S^* t] = 1 + \mathcal{L}_S^* t + \mathcal{O}(t^2)$ provides a microscopic expression for the *short-time* collective diffusion coefficient, $D_c^s(k) = D_c(k,t\to 0)$. On one hand, $F_c(k,t) = S(k) - k^2 D_c^s(t=0)t + O(t^2)$ and also from Eq. (11) $F_c(\mathbf{k},t) = S(\mathbf{k}) + \langle\rho(\mathbf{k}^*)\hat{\mathcal{L}}_S^*\rho(\mathbf{k})\rangle t + O(t^2)$ so $D_c^s(k) = k^{-2}\langle\rho(\mathbf{k}^*)\hat{\mathcal{L}}_S^*\rho(\mathbf{k})\rangle$. After some simple algebra one concludes[2]

$$D_c^s(k) = D_0\frac{H(k)}{S(k)}, \tag{13}$$

with $H(k)$ the hydrodynamic mobility function,

$$H(k) = \frac{1}{N}\sum_i\sum_j\left\langle \hat{\mathbf{k}}\cdot\frac{\mathbf{D}_{ij}(\mathbf{q})}{D_0}\cdot\hat{\mathbf{k}}\exp[-i\mathbf{k}\cdot(\mathbf{q}_j-\mathbf{q}_i)]\right\rangle, \tag{14}$$

which involves the microscopic diffusion matrix $\mathbf{D}_{ij}$ between pairs. In this work, we focus on wave vectors in the confining plane $(x-y)$, i.e., $\mathbf{k}\cdot\mathbf{z} = 0$. The hydrodynamic mobility is usually decomposed as $H = H_s + H_c$ where the self-contribution H_s corresponds to $i = j$ in Eq. (14) and the cross contribution H_c to $i \neq j$. The self-contribution involves self-diffusion $\mathbf{D}_{11}(\mathbf{q})$, which depends on the reflections of the hydrodynamic perturbations impinging in the rest of the particles and coming back to the tagged particle. Therefore, the hydrodynamic contribution to the self-diffusion becomes important at short distances $\mathbf{D}_{11} = 1 + O(a/r)^4$ and reduces the self-diffusion coefficient D_c from the bare free diffusion in dilute suspension, as the colloidal surface fractions increases, $D_s = D_0(1-\alpha_s\phi)$, where α_s also depends on the interparticle potential [17].

Here we are more interested in the collective cross-diffusion, which corresponds to Eq. (14) for $i \neq j$. For distant particles i and j, the microscopic mutual diffusion can be approximated by the celebrated Oseen tensor,

$$\mathbf{D}_{ij}(\mathbf{q}_{ij}) = D_0\frac{3}{4}\frac{a}{r}(\mathbf{1} + \hat{\mathbf{q}}_{ij}\hat{\mathbf{q}}_{ij}), \tag{15}$$

with $D_0 = k_B T/(6\pi\eta a)$ the Stokes-Einstein relation. $\hat{\mathbf{q}}_{ij} = \mathbf{q}_{ij}/q_{ij}$ is a normalized vector and $\mathbf{q}_{ij} = \mathbf{q}_j - \mathbf{q}_i$. The Oseen expression is a pairwise approximation to the colloid diffusivity, which enables us to split the ensemble average of Eq. (14) as $N(N-1)\sim N^2$ equivalent integrals involving pairs. This permits us to write

$$H_c(k) = N\int P_2(\mathbf{q}_1,\mathbf{q}_2)\hat{\mathbf{k}}\cdot\frac{\mathbf{D}_{12}(\mathbf{q}_{12})}{D_0}\cdot\hat{\mathbf{k}} \times \exp[-i\mathbf{k}\cdot\mathbf{q}_{12}]d\mathbf{q}_1 d\mathbf{q}_2, \tag{16}$$

where the reduced probability $P_2(\mathbf{q}_1,\mathbf{q}_2) = \int d\mathbf{q}_3,\ldots,\mathbf{q}_N P(\mathbf{q})$ has been introduced to collect the integration over dummy coordinates.

Expression (16) can be analytically evaluated using the Oseen tensor approximation for the microscopic mobility of confined suspensions and under the dilute limit. In this dilute limit P_2 can be approximated by

$$P_2(\mathbf{q}_1,\mathbf{q}_2) = \frac{1}{\mathcal{Z}_2}\exp\{-\beta[\Psi(q_{12}) + V(z_1) + V(z_2)]\}, \tag{17}$$

where $\Psi(q_{12})$ is the interaction potential between the generic particles 1 and 2 and $V(z)$ is the external confining potential acting on each particle $V(z) = (1/2)k_s z^2$. Solving integrals 16 for the cases of ideal colloids (Appendix A),

$$H_c(k) = 3\phi\frac{\delta}{a}\left\{\left[\frac{1}{2}(k\delta)^{-1} + (k\delta)\right]e^{(k\delta)^2}\mathrm{erfc}(k\delta) - \frac{1}{\sqrt{\pi}}\right\}. \tag{18}$$

As expected, the hydrodynamic function is governed by the nondimensional group $k\delta$, where $\delta = (k_B T/k_s)^{1/2}$ is the confinement width. We now present results and discuss the

[2]For any two phase functions $a = a(\mathbf{q})$ and $b(\mathbf{q})$ partial integration leads to $\langle a(\mathbf{q})\hat{\mathcal{L}}_S^* b(\mathbf{q})\rangle = -\langle\nabla_q a\cdot\mathcal{M}(\mathbf{q})\cdot\nabla_q b\rangle$.

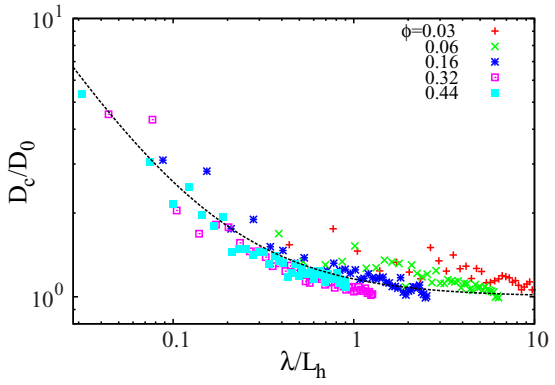

FIG. 2. Hydrodynamic function versus the the ratio L_h/λ for ideal colloids at various densities. The hydrodynamic length is $L_h = (\frac{2}{3\phi})a$ with ϕ the colloidal surface fraction and a the colloid radius. Dashed line shows $D_c/D_0 = 1 + \frac{1}{2\pi}(\lambda/L_h)$.

different regimes: strict 2D confinement $k\delta \ll 1$ and soft confinement $k\delta \sim 1$ and transition to normal 3D diffusion $k\delta \gg 1$.

III. STRICT 2D CONFINEMENT: $\delta \to 0$

A. Ideal tracers

For $k\delta \ll 1$, wavelengths much larger than the confining width, Eq. (18) recovers the result for the strict 2D confinement derived in Ref. [10], leading to anomalous enhancement of collective diffusion $D_c \sim k^{-1}$,

$$\lim\ k\delta \to 0 \qquad H_c(k) = \frac{\rho_{2D}}{4\mu_0\eta}k^{-1} = \frac{1}{L_h k}. \tag{19}$$

We have introduced the bare free particle mobility $\mu_0 = (6\pi\eta a)^{-1}$ and a characteristic hydrodynamic length,

$$L_h = \frac{2}{3\pi}\frac{1}{\rho_{2D}a} = \left(\frac{2}{3\phi}\right)a, \tag{20}$$

under the 2D-confinement case. Hydrodynamic couplings becomes relevant for collective diffusion for wavelengths larger than L_h. Expressing L_h in terms of the surface fraction ($\phi < 1$) clearly reveals that L_h is somewhat smaller but of the order of the colloid size a so hydrodynamic enhancement become relevant even at moderate wavelengths. By collecting terms in Eqs. (13) and (14) one concludes that

$$\frac{D_c}{D_0} = 1 + \frac{1}{L_h k}, \tag{21}$$

meaning that at long wavelengths $kL_h < 1$, collective diffusion becomes much faster than self-diffusion. According to Eq. (20), the hydrodynamic length L_h is inversely proportional to the particle surface fraction $L_h \sim \phi^{-1}a$. A series of simulations increasing the number of ideal colloids indeed verifies this relation. Figure 2 compares Eq. (21) with simulations obtained for a large range of colloid densities, plotted in the master curve $D_c(k)/D_0$ against λ/L_h (with $\lambda = 2\pi/k$ wavelength of the density fluctuation).

Equation (21) means that under 2D confinement, long colloid density fluctuations are homogenized much faster than one would expect from normal diffusion. The time required to homogenize an initial density perturbation with small wave number k is $\tau_k = [k^2 D_c(k)]^{-1} \sim L_h/(kD_0) = (2/3\phi)[\tau_0/(ka)]$, where $\tau_0 = a^2/D_0$ is the colloid diffusion time. Over this time τ_k one single colloid has diffused a distance l, given by $l/a \sim (\lambda/a)^{1/2}(4\pi/3\phi)^{1/2}$. As λ is made larger, this distance l becomes much shorter than the inhomogeneity of the density perturbation λ. This strongly contrasts with normal diffusion, because in this case the particle would have diffused a distance $l \sim \lambda$ in a time $\tau_k \sim (k^2 D_0)^{-1}$, which is what one certainly expects if the initial density inhomogeneity is to be blurred away.

The origin of this apparent paradox is the coordinated motion induced by hydrodynamic forces over the manifold where colloids move. To illustrate this we made a simulation where a collection of neutral colloids where initially placed forming three large density stripes, see Fig. 3. We then measured the rate at which these patterns spread and studied the effect of hydrodynamics by comparison between HI and Brownian dynamics (BD) simulations without hydrodynamics. Under the presence of HI, collective diffusion drives individual colloids towards less-populated regions, faster than self-diffusion does. The vast majority of research on diffusion in 2D confined environments (such as membrane lipids [18] and membrane proteins [19]) focus on the mean-squared displacement (MSD) of individual elements. However, as shown in Fig. 3, no signature of hydrodynamic enhanced collective diffusion can be detected in the MSD of a single colloid, which is the same result as for independent Brownian walkers. In real space, the enhanced collective diffusion is clearly revealed in the van Hove function [20], here projected according to the symmetry of the stripes,

$$G(x,t) = \frac{1}{N}\left\langle \sum_{i,j} \delta[x - x_i(t) + x_j(0)] \right\rangle, \tag{22}$$

which can be decomposed in self ($i = j$) and collective ($i \neq j$) parts $G(x,t) = G_s(x,t) + G_c(x,t)$. Both contributions to G are plotted in Fig. 3(d) for $t = 20a^2/D_0$. The self part of the van Hove function is similar for HI and BD simulations. This is also revealed in the MSD of a single neutral colloid shown in Fig. 3(c), where for $t > \tau_D = a^2/D_0$, HI and BD results perfectly match. Hydrodynamic interactions do not alter the self-diffusion of neutral colloids because ideal tracers simply do not perturb the fluid. By contrast, the collective part G_c broadens significantly when HI are present, regardless of colloid-colloid interactions (in these simulations we consider neutral colloids). The time evolution of the mean-squared width of the stripes plotted in Fig. 3(b) clearly illustrates a faster collective diffusion induced by HI.

B. Effects of colloidal short-range interactions

Colloids with steric or potential interactions might present two different diffusion regimes at large colloid densities. While the short-time diffusion arises from local colloidal motions, the long-time diffusion is smaller and represents many escapes [of individual colloid (self-diffusion) or of collective patterns] out from the "molecular cages" or "energy traps" created by surrounding neighbors. Here we considered two types of short-range interactions: a purely repulsive potential (WCA) and a Lennard-Jones-type attractive potential (LJ). None of

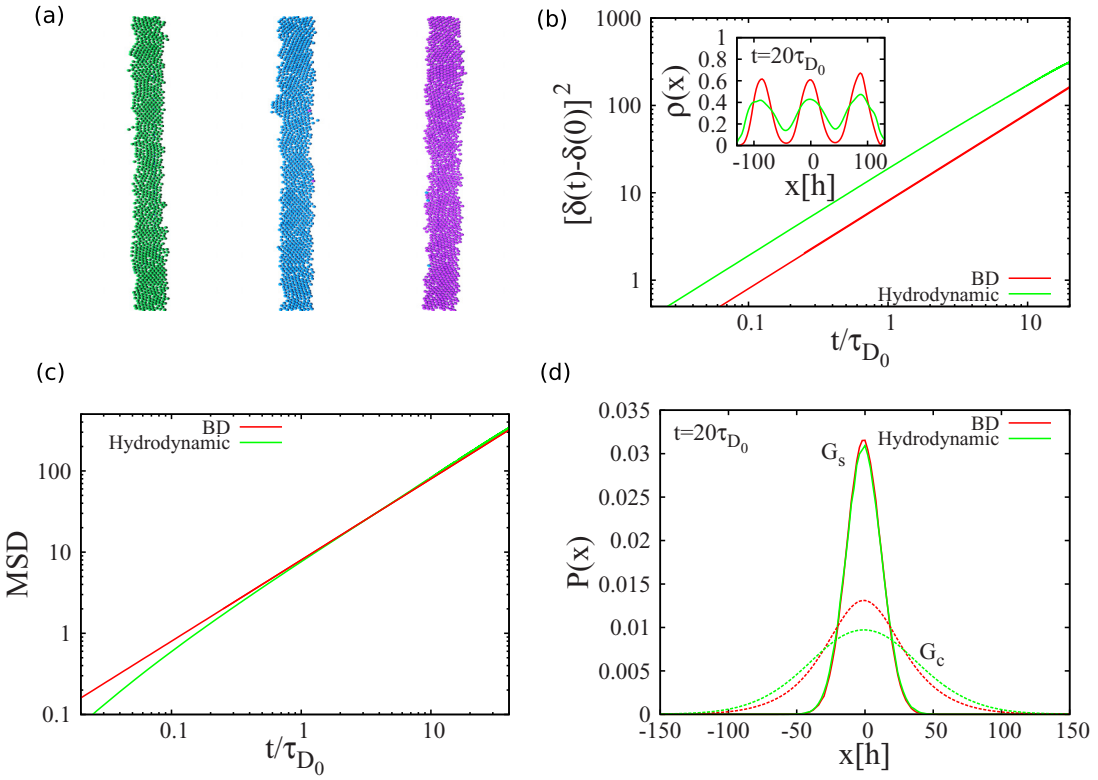

FIG. 3. (a) Initial density pattern with stripes. (b) The evolution of the stripes' mean-squared width and (inset) the density profiles at $t = 20\tau_D$ (with $\tau_D = a^2/D_0$) comparing cases with and without (BD) hydrodynamics. (c) The mean-squared displacement of one colloid (note that HI's have a negligible effect on self-diffusion). (d) The self $G_s(x)$ and collective $G_c(x)$ parts of the van Hove function for $t = 20\tau_D$, comparing results with and without hydrodynamics.

these systems were observed to present different diffusion regimes at different times, at least for surface fractions in the range $\phi \leqslant 0.6$. This is illustrated in Fig. 4, where we show the collective intermediate scattering function $F_c(k,t)$ and (in the inset) the self-diffusion coefficient, obtained from the mean-squared displacement of a colloid. At any wave number considered, the density-density correlation $F(k,t)$ decays exponentially, with one only characteristic decay rate,

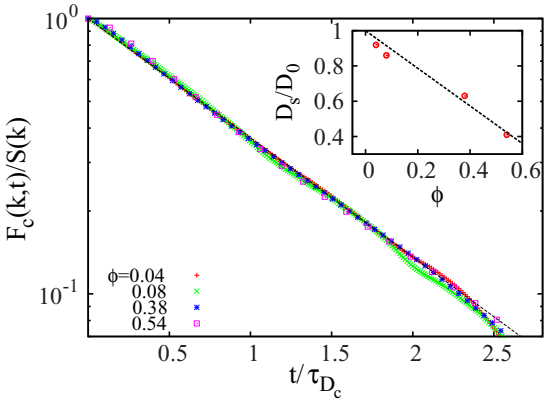

FIG. 4. Intermediate collective scattering function $F_c(k,t)$ for a system of WCA colloids versus the scaled time t/τ_{D_c} with $\tau_{D_c} = k^2 D_c(k)$. The inset shows the self-diffusion coefficient against the surface fraction $\phi = \pi a^2/L^2$, the dashed line corresponds to $D_s = D_0(1 - 1.07\phi)$.

$k^2 D_c(k)$. This means that short and long collective diffusion coincide, $D_c^s = D_c^l$.

As shown in Eq. (13), conservative forces enter in the collective diffusion via the static structure factor $S(k)$, which is completely flat for ideal colloids $S(k) = 1$. Depending on the interaction potential, the effect of the static fluid structure might reach relatively small wavelengths masking the hydrodynamics of anomalous collective diffusion enhancement. For these short-range potentials, the effect of the fluid order reaches about 3 times the particle diameter. To illustrate the effect, Fig. 5(top) compares simulations with and without hydrodynamic interactions. Only at the largest wave numbers could we observe deviations between HI and BD results for $D_c(k)$, resulting from the hydrodynamic enhancement of $H(k) \sim k^{-1}$. This "masking" of the fluid structure might induce inaccuracies in the evaluation of the divergence exponent of the collective diffusion under experimental conditions [12]. Figure 5(b) shows the hydrodynamic function $H(k)$ against kL_h for different densities of WCA colloids, illustrating the transition to the enhanced diffusion at low k. At molecular wavelengths the collective diffusion is heavily influenced by the fluid structure but *also* by HI. While the effect of short-range HI's has been extensively studied in the 3D space, there is not much information about how HI's influence the mobility of close colloids under confinement. Variations in near-field mobilities might be relevant for aggregation processes and colloid detachment (breaking of physical bonds). Here we briefly explore this

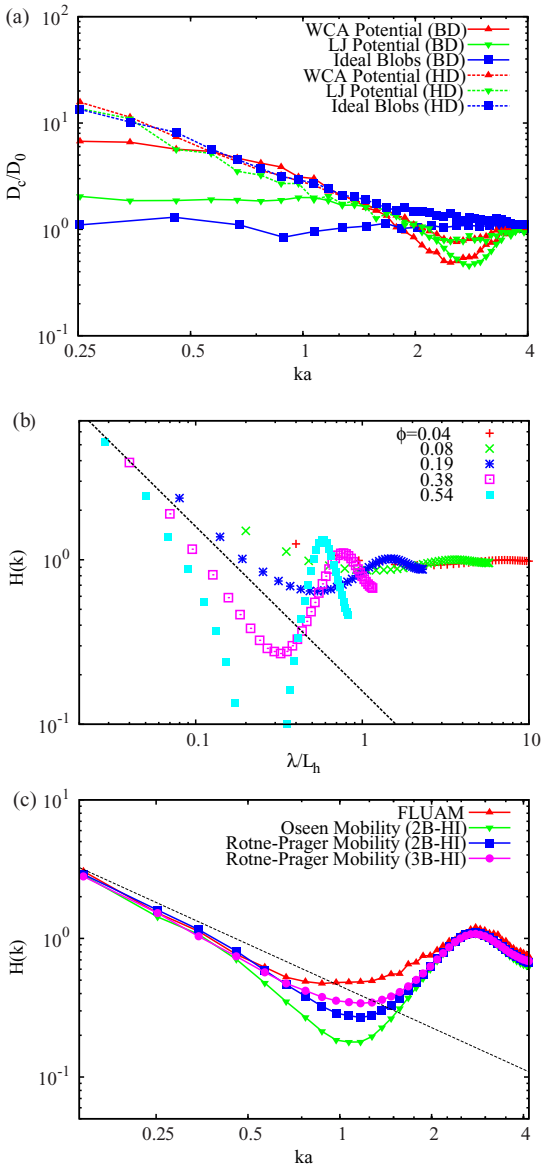

FIG. 5. (a) Collective diffusion coefficient at surface fraction $\phi = 0.38$. Solid and dashed lines respectively correspond to BD (non-HI) and HI simulations. Symbols denote different colloidal interactions: ideal colloids (squares), WCA (top triangles), and LJ (down-triangles). (b) The hydrodynamic function $H(k)$ versus the the ratio λ/L_h for colloids interacting with the WCA potential at different densities. Dashed line shows the asymptotic behavior $H(\lambda/L_h) \propto (\lambda/L_h)^{-1}$. (c) $H(k)$ for WCA colloids at surface fraction $\phi = 0.38$ and different mobility kernels. Calculations were done by averaging using Eq. (14) over many colloid equilibrium configurations obtained from simulations B 1. Dashed line indicates the asymptotic behavior $H(ka) \propto (ka)^{-1}$.

effect by comparing an approximation of pairwise mobility with the corresponding three-body contribution. Three-body contributions to the mobility arise from the reflections of the fluid perturbative flow on each particle surface. Here, we estimate three-body effects by inserting in H_c [Eq. (14)] the formulas for two- and three-body contributions to hard spheres mobility at the level of the Rotne-Prager approximation (see Dhont's book [17]). The comparison, shown in Fig. 5(bottom) indicates that three-body effects increase the mobility of near-by colloids at distances slightly larger than their diameter. Figure 5(c) also includes the mobility obtained using the Oseen tensor, which is a valid description for large distances, as can be seen from the convergence of all mobilities at small k. For reference, Fig. 5 also includes a direct evaluation of $H_c(k)$ from simulations, obtained on Eq. (13) and independent evaluations of dynamics $D_c(k)$ and structure $S(k)$. Note that the blob model we used here does not take into account the particle rigidity (stresslet) and cannot include three-body effects (these would require multiblobs with rigid constraints [21] or springs [22]). Figure 5(bottom) shows that for $k > 2$, the collective diffusion is controlled by molecular interactions [the $D_c(k)$ is basically the same for all the mobilities considered]. Notably, the most sensible region for $D_c(k)$ in terms of hydrodynamic details (mutual mobility kernel) corresponds to distances of between 4 and 1.5 particle diameters (i.e., $0.5 < k < 2$).

IV. SOFT CONFINEMENT: TRANSITION TO NORMAL DIFFUSION

For wavelengths of the order of the confinement width δ or smaller, Eq. (20) recovers the normal diffusion regime which for ideal colloids is just $H_c = 0$,

$$\lim\ k\delta \gg 1, \qquad H_c(k) \to 0. \tag{23}$$

Simulations for ideal colloids at fixed density and varying intensity of the confining potential were performed to validate the prediction of Eq. (18). Results, shown in Fig. 6, indicate an excellent agreement between theory and simulations, revealing the gradual transition from enhanced 2D collective diffusion to normal 3D diffusion taking place around $k\delta \sim 1$. The "2D" and "3D" nature of the collective diffusion regime is has been indicated in Fig. 6.

To further investigate the details of this gradual transition from 3D- to 2D-dominated collective diffusion, we analyzed the average hydrodynamic force felt by two columns of colloids (in the z direction) separated by a distance s in the confining plane. In the strict confinement case (colloids constrained to move in the $z = 0$ plane, i.e., "columns" of zero height) such collective hydrodynamic drag is repulsive and

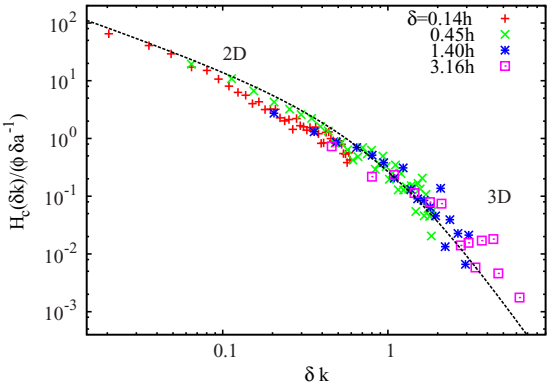

FIG. 6. Collective diffusion under a soft Gaussian trap of width δ, see Eq. (1). Results correspond to ideal colloids at surface fraction $\phi = 0.6$. The simulation box is $128 \times 128 \times 100h^3$, where h is the fluid grid size (see Sec. B 1). The dashed line correspond to Eq. (18).

proportional to $1/s^2$ [13]. We denote the location of particle i as $\mathbf{r}_i = \mathbf{s}_i + z_i\hat{\mathbf{z}}$ with $\hat{\mathbf{z}}$ the unit vector in the z direction. The average hydrodynamic force on a tagged colloid $i = 1$ due to a colloid $i = 2$ is $\mu_0\mathbf{v}_{21} = \mathcal{M}_{12}\mathbf{F}_2$, with $\mathcal{M}_{12}$ the mutual mobility. The force on particle "2" is uniquely determined by the confining potential (ideal particles) so $\mathbf{F}_2 = -k_s z_2\hat{\mathbf{z}}$. The total force on the column located at $\mathbf{s_1}$ due to another column of colloids at $\mathbf{s}_2$ is obtained by integrating over z_1 and z_2,

$$\mathbf{f}_{21}(s) = \mu_0^{-1}\int dz_1\int dz_2 P_2(\mathbf{r}_1,\mathbf{r}_2)\mathcal{M}_{12}(\mathbf{r}_2-\mathbf{r}_1)\mathbf{F}_2(\mathbf{r}_2), \tag{24}$$

where we note that the distance $|\mathbf{s}_1 - \mathbf{s}_2| = s$ is fixed and that $\mathbf{s} = \mathbf{s}_2 - \mathbf{s}_1$ points towards $\mathbf{s}_2$. Using the modified coordinates $Z = (z_1 + z_2)/2$ and $z = (z_1 - z_2)$ and working out the two-particle probability P_2 (which only depends on z coordinates, see Appendix A) one gets,

$$\mathbf{f}_{21} = -\frac{3k_s a}{8\sqrt{\pi}}\int_{-\infty}^{\infty} d\tilde{z}\exp\left[-\frac{\tilde{z}^2}{4}\right]\frac{\tilde{z}^2}{(\tilde{s}^2+\tilde{z}^2)^{3/2}}\,\tilde{\mathbf{s}}, \tag{25}$$

where $\tilde{\mathbf{s}} = \mathbf{s}/\delta$ and $\tilde{z} = z/\delta$ are scaled distances in the plane from column 1 to column 2 and in height. The integral can be evaluated to finally provide

$$\mathbf{f}_{21} = k_s a\mathcal{F}(\tilde{s})\,\hat{\mathbf{s}}, \tag{26}$$

$$\mathcal{F}(s) = \frac{3s}{32\sqrt{\pi}}\exp[s^2/8]\left[(s^2+4)K_0\left(\frac{s^2}{8}\right) - s^2K_1\left(\frac{s^2}{8}\right)\right], \tag{27}$$

where K_0 and K_1 are modified Bessel functions of the second kind and $\hat{\mathbf{s}}$ an unit vector in the plane.

The mutual force $f_{21} \sim k_s a$ is proportional to the confining "spring constant" in the z direction, k_s, meaning that the enhancement of mutual diffusion dies out gradually as the confinement is made softer, as one should expect. More interesting is the dependence of $\mathbf{f}_{21}$ with the in-plane distance s, which is plotted in Fig. 7.

The hydrodynamic force (on column 1) is repulsive (pointing away from column 2) and reaches a maximum value at $s_{\max} \simeq 0.667\delta$. For $s > s_{\max}$ the repulsive force decays like $1/s^2$, like in the strict confinement case. However, for $s < s_{\max}$ the mutual hydrodynamic "repulsion" also dies out gradually as $s \to 0$ (like $f_{21} \sim s\log(s)$). This second regime corresponds to parcels of colloids which are so close (with respect the confinement width δ) that they tend to behave as if they were in 3D (where $f_{21} = 0$). Beyond the column-column interaction, one could analyze in deeper detail the structure of mutual mobility field inside the layer. In particular, we analyze the force due to a column of colloids at $\mathbf{s}$ on a colloid $i = 1$ at $\mathbf{s}_1 = 0$ and at height z_1. The components of such force in $\hat{\mathbf{s}}$ (pointing towards the column) and the $\hat{\mathbf{z}}$ directions are

$$\mathbf{f}\cdot\hat{\mathbf{s}} = -\frac{3k_s a}{4\sqrt{2\pi}}\int_{-\infty}^{\infty} d\xi\,\frac{\exp[-(\tilde{z}_1+\xi)^2/2]\,\tilde{s}\xi(\tilde{z}_1+\xi)}{(\tilde{s}^2+\xi^2)^{3/2}}, \tag{28}$$

$$\mathbf{f}\cdot\hat{\mathbf{z}} = -\frac{3k_s a}{4\sqrt{2\pi}}\int_{-\infty}^{\infty} d\xi\,\frac{\exp[-(\tilde{z}_1+\xi)^2/2]}{(\tilde{s}^2+\xi^2)^{1/2}} \times\left[1+\frac{\xi^2}{(\tilde{s}^2+\xi^2)}\right](\tilde{z}_1+\xi), \tag{29}$$

with $\tilde{z}_1 = z_1/\delta$ and $\xi \equiv (z_2 - z_1)/\delta$. This force field, illustrated in Fig. 7(b), indicates that the hydrodynamic force exerted by the the column becomes attractive if the colloid is far enough from the layer center $|z| > O(\delta)$. This counterflow, shown in Fig. 7(b), is the signature of the Oseen tensor within the finite layer and it is the origin of the gradual slowdown of collective diffusion as the confinement is made softer $\delta \gg a$.

A pertinent question is how does the strict confinement (or in mathematical terms holonomic constraint) is recovered as the confining potential becomes infinitely stiff. The current at $\mathbf{r}_1$ is $\mathbf{v}_1 = \int d\mathbf{r}_2 P(\mathbf{r}_2)\mathcal{M}_{12}(\mathbf{r}_1,\mathbf{r}_2)\mathbf{F}(\mathbf{r}_2)$ and we have $\mathbf{F}_2 = -\nabla_{\mathbf{r}_2}U$ and $P(\mathbf{r}_2) \propto \exp[-\beta U(\mathbf{r}_2)]$. Thus $\mathbf{v}_1 = \int d\mathbf{r}_2\mathcal{M}_{12}\nabla_{\mathbf{r}_2}P = -k_BT\int d\mathbf{r}_2 P(\mathbf{r}_2)\nabla_{\mathbf{r}_2}\cdot\mathcal{M}_{12}$. For $\beta k_s \to \infty$, $P(\mathbf{r})$ becomes a Dirac δ (in our case it forces $z_2 = 0$) and one gets the known limit [13] $\mathbf{v}_1 = -k_BT\nabla_{\mathbf{r}_2}\cdot\mathcal{M}_{12} = k_BT\nabla_{\mathbf{r}_1}\cdot\mathcal{M}_{12}$, where $\mathbf{r}_i$ is constrained to move over some manifold (here $z_i = 0$).

Equation (18) can be used to determine the minimum wavelength $\lambda = 2\pi/k$ required for collective diffusion to

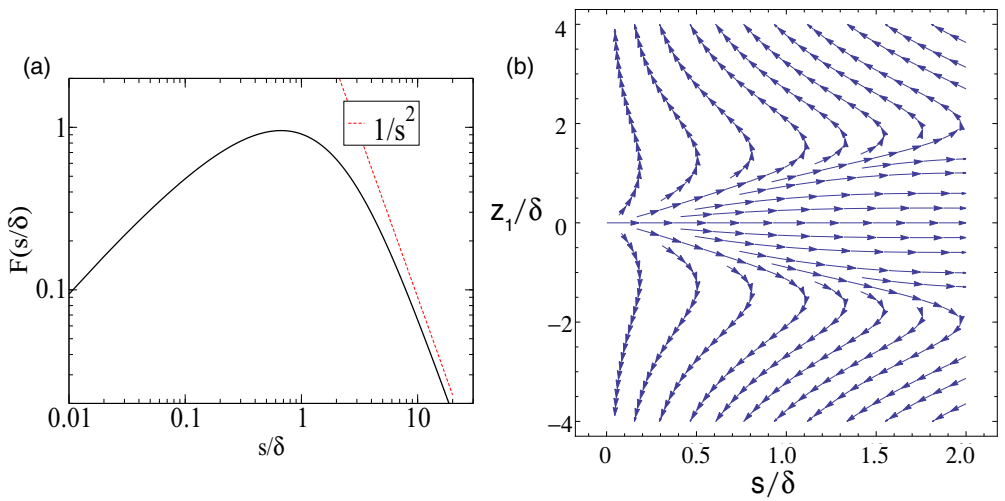

FIG. 7. (a) The magnitude of the force in Eq. (26), between two columns of colloids separated by an in-plane distance s. (b) The hydrodynamic force field on a single colloid at height z_1 due to a colloid column at distance s.

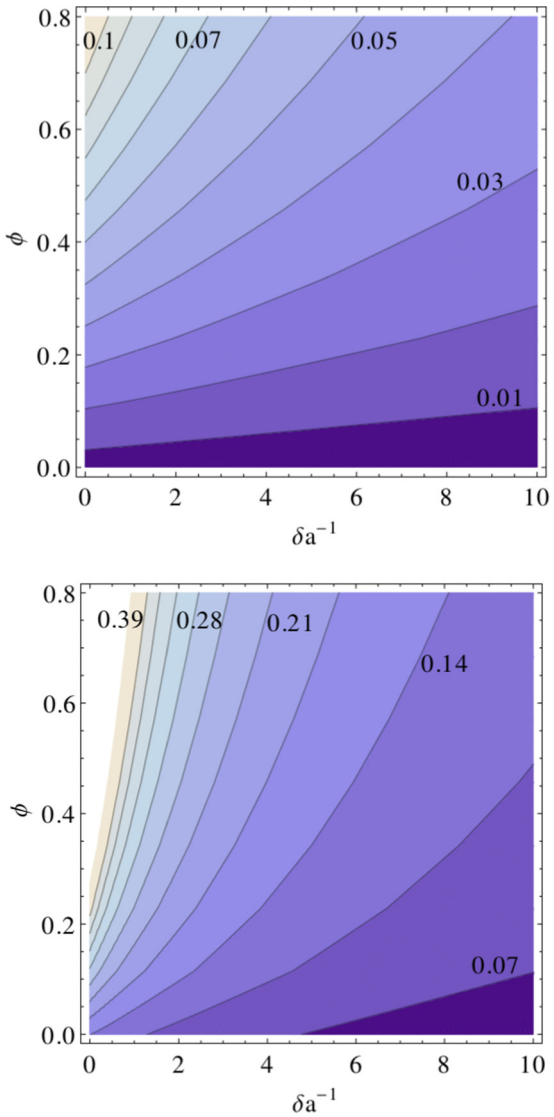

FIG. 8. Contour plots of the wave number ka (with a the particle radius) at which the hydrodynamic function equals $H_c(k) = 10$ (a) and $H_c(k) = 1$ (b). According to Eq. (13) both cases respectively correspond to D_c 2 times and more than 10 times faster than D_0.

become significantly larger than in an unbounded 3D domain. The corresponding wave number $k = k(\mathcal{H})$ is the solution of the transcendental equation $H_c(k) = \mathcal{H}$ arising from Eq. (18). We recall that $H = H_s + H_c \simeq 1 + H_c$, so if $H_c(k) = 1$ the collective diffusion $D_c(k) = D_0 H(k)/S(k)$ is approximately doubled with respect diffusion in unbounded 3D domain. Figure 8 shows the wave-number isocontours for $H_c(k) = 1$ (left) and $H_c(k) = 10$ (right) in a surface fraction ϕ-confinement δ chart. As an example, for a projected surface fraction ($\phi = \pi a^2 N/L^2$) of about 0.4, a rather soft confining potential of width $\delta = 3a$ will induce more than a 10-fold increase in collective diffusion ($H_c = 10$) for a wavelength $\lambda \sim 100\,a$. For nanoparticles (of about 10 nm) these lengths are still small (order 10 microns). The effect is somewhat reduced in dilute suspensions, as for $\phi = 0.1$, one would require system sizes or patterns with $\lambda \simeq 400\,a$ to observe a 10-fold increase in $D_c(\lambda)$. There are many applied examples where these observations are relevant, in general, cases where colloids are confined near a wall or by some external potential. For charged colloids near charged surfaces, the Debye length (here acting as δ) can be quite small (nanometers). Colloids can be softly attracted to walls in polymer-colloid mixtures due to depletion forces; in this case $\delta \sim a$. In these two cases, the mobility gradient is also modified by the wall presence. An example where the present theory is directly applicable is colloidal confinement by ultrasound. The ultrasound (quadratic) potential arising from high-frequency (MHz) pressure waves and matter interaction allows us to confine colloids in strips of quite small width (typically $\delta \simeq a$ for colloid radius a in the micron range) [6,7,23].

V. CROSSOVER TO THE INERTIAL REGIME

An immediate striking consequence of the divergence of the collective diffusion $D_c \propto k^{-1}$ is that, for a small-enough wave number, mass diffusion becomes faster than vorticity diffusion and inertia. This wave number determines a crossover between overdamped and damped (oscillatory) density fields. A simple estimation can be obtained from the ratio between mass and vorticity diffusion characteristic times [respectively, $\tau_{D_c} = (D_c k^2)^{-1}$ and $\tau_\nu = (\nu k^2)^{-1}$] providing

$$k_c a \ll \frac{3}{2}\phi\frac{1}{\mathrm{Sc}}. \tag{30}$$

The Schmidt number for a small 10-nm colloid is already a huge number $\mathrm{Sc} \sim 10^7$, so the crossover would be only possibly observed at macroscopic lengths (millimeters to centimeters). We now present a numerical study of the transition to the damped regime and compare with theoretical results of Dominguez *et al.* [14]. To make the transition wavelengths accessible to simulations, we consider unrealistically small values of Sc in our time-dependent scheme (which includes advection and transient terms in the fluid momentum equation). The analysis of Dominguez *et al.* [14] provides the expression for the time evolution of the intermediate scattering function obtained by preserving the transient and advective terms in the fluid momentum equation,

$$F_c(k,t) = S(k)\left\{\frac{4}{3}e^{-\frac{u}{2}t}\cos\left(\frac{\sqrt{3}}{2}ut\right) - \frac{1}{\pi}\int_0^\infty dx\,\frac{\sqrt{\pi}}{x^3+1}e^{-utx}\right\}, \tag{31a}$$

$$u = \left[\frac{4\rho_f\eta}{(k_bT)^2\rho_{2D}^2}\right]^{-\frac{1}{3}}k^{4/3}. \tag{31b}$$

Equation (31a) present a damped oscillatory behavior with a frequency where $\tau_D = (k^2 D_0)^{-1}$. The frequency u increases algebraically with $k^{4/3}$ due to the advection of the ambient flow. In deriving these relations, Dominguez [14] used the $k \to 0$ limit to approximate the Green function. This approximation is correct for very large wavelengths and basically neglects the diffusion of solvent momentum in the plane (which scales like k^2) in favor of the transient advection ($\partial_t v$).

Figures 9(a) and 9(b) illustrate the change in dynamic regime by comparing the collective scattering function obtained for $kh = 0.05$ and $kh = 0.12$ and for large and small values of the Schmidt number ($\mathrm{Sc} = 900$ and $\mathrm{Sc} = 5$). The

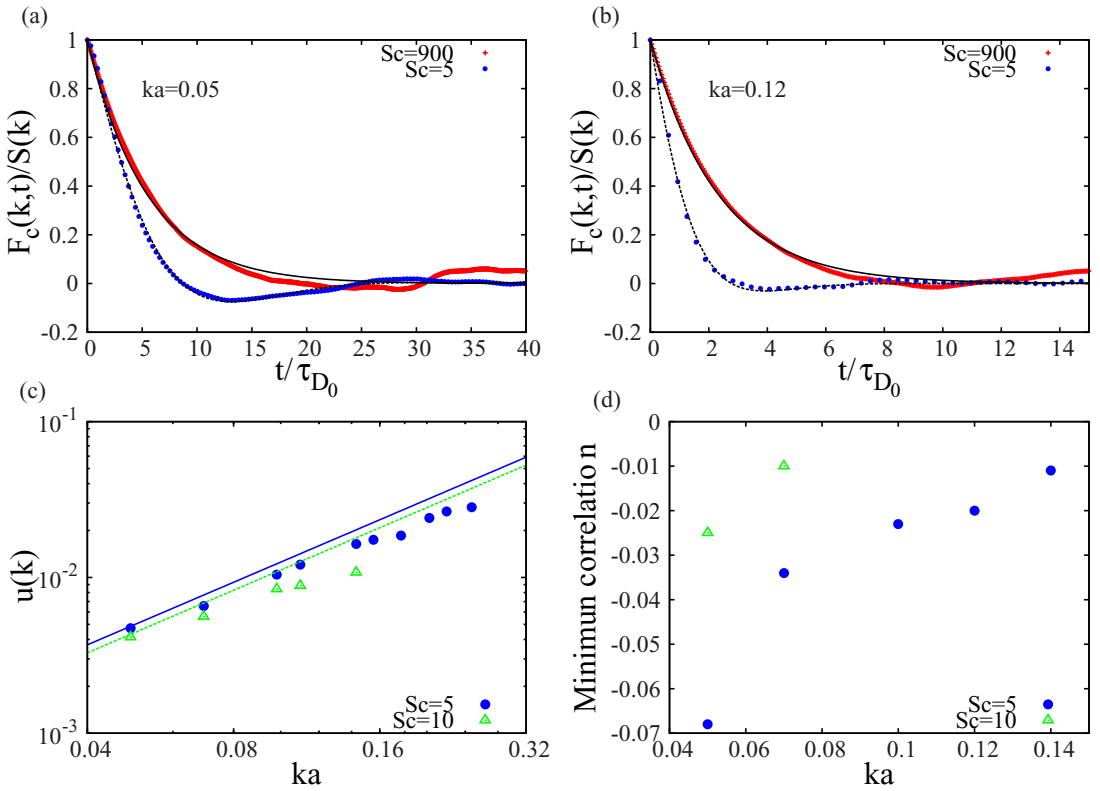

FIG. 9. Normalized collective intermediate scattering function of ideal tracers at wave numbers $kh = 0.05$ (a) and $kh = 0.12$ (b) for two different Schmidt numbers (h is the mesh size). Time is scaled with the particle diffusion time $\tau_{D_0} = a^2/D_0(\mathrm{Sc})$, where the Schmidt dependence of $D_0(\mathrm{Sc})$ was taken from Ref. [24]. (c) Values of the frequency $u(k)$ obtained from best fit of simulation results to Eq. (31a). (d) The minimum (negative) value of the normalized collective intermediate scattering function $F_c(k,t)/S(k)$. Lines corresponds to analytic result in Eq. (31a) and Eq. (31b). In all cases the box dimensions are $128 \times 128 \times 100\,h^3$ and the surface fraction $\phi = 0.6$. The values of the crossover wave number k_c in Eq. (30) are $0.18/h$, $0.09/h$ and $0.001/h$, respectively, for Sc = 5, 10, and 900.

large value of Sc (red symbols) is clearly in the overdamped regime $k > k_c = 0.001h^{-1}$ [see Eq. (30)] and it is in excellent agreement with the overdamped expression for $F(k,t)$ in Eq. (7) (solid line in Fig. 9). The crossover wave number for Sc = 5 is $k_c = 0.18h^{-1}$ and thus for $k = 0.05/h < k_c$ we are now exploring the inertial regime. Simulations indeed show damped dynamics with a negative correlation in the density correlation $F_c(k,t)$ at some finite time (of about 10 bare diffusion times, $\tau_D = a^2/D_0$). Figure 9(b) shows the case $k = 0.12\,h^{-1}$ which is still below the crossover $k_c = 0.18\,h^{-1}$ for Sc = 5. In this case, the peak of negative correlation is quite small, indicating that the dynamic is almost overdamped. In Fig. 9(c) the dashed line corresponds to the best fit to the theoretical expression in Eq. (31a), using the frequency u appearing in Eq. (31a) as only free parameter. The agreement with the theory is excellent for this value of k. This is also illustrated in Fig. 9(c) where the numerical estimations of $u(k)$ obtained from best fits to Eq. (31a) are compared with the theoretical expression for the frequency $u(k)$ in Eq. (31b). However, for slightly larger values of k_c simulations start to systematically deviate from the theory. This fact can be seen in Fig. 9(c), showing that the theoretical trend $u(k) \propto k^{4/3}$ is not recovered for $k > k_c/4$. The relative difference of $u(k)$ with respect the theoretical value reaches about 25% for $k \simeq k_c$ and decreases to about 3% for $(k_c - k) \simeq 0.7k_c$. Deviations from the theory as k increases were to be expected because the theory was developed using the $k \to 0$ approximation for the Green function (mobility) [14].

VI. CONCLUSIONS

We have analytically derived and numerically studied the collective diffusion of colloids under a confining quadratic potential, corresponding to a Gaussian trap of width δ. This setup permits us to determine how robust is the hydrodynamic effect which is known to enhance the collective diffusion of large wavelength patterns of colloidal density when colloids are trapped in a 2D surface embedded in the surrounding 3D fluid. The excellent agreement between analytical and numerical results permits us to conclude that the anomalous enhancement of collective diffusion is robust and still significant under soft confinement. For instance, that a stain of a couple of microns formed by a concentrated phase of nanocolloids of size $a = 2.5$ nm (to put the typical size of a protein) softly trapped ($\delta \simeq 2a$) near a surface (e.g., by electrostatic or depletion forces) will spread towards less-populated regions 10 times faster than by the "standard" diffusion. The effect is more important at large surface fractions, for instance, for $\phi \simeq 0.5$, a very slight confinement with $\delta \sim 10a$ still enhances in about 10-fold the collective diffusion of wavelengths $\lambda \sim 150a$. We believe that the consequences of this hydrodynamic effect are relevant in transport phenomena in biological systems

and nanotechnological applications. This work highlights the need of considering collective diffusion when studying Brownian displacements of colloids or molecules restricted to move in a manifold embedded in a higher dimensionality. The list of environments is large [14,25] and includes vesicles, lipids, or proteins in membranes; colloids near charged surfaces with DLVO forces; or depletion. In fact, the hydrodynamic enhancement of collective diffusion is scarcely being taken into account in applied studies. After the first experimental evidence of the phenomena [26], an increasing number of groups have been or are now involved in studying different scenarios involving hydrodynamics in confined geometries [2,12,14,16,25]. Renewed experimental interest have showed even larger diffusion enhancement under quasi-1D confinement [11], which is relevant for the collective diffusion of molecular motors moving in molecular filaments. Collective diffusion determines the spreading of patterns created by a collection of diffusing individuals. In confined media, hydrodynamics not only enhance spreading but also probably activate their coordinated motion. This is particularly relevant for systems like lipid rafts [27] and motor proteins walking over microtubules [28,29], where the origins of the observed coordinated motions are still under scrutiny.

Another aspect of this work has been a validation of Dominguez's theory [25] for the inertial regime at very small wave numbers. Simulations were performed at unphysical values of the Schmidt number to be able to explore the inertial regime, which takes place for $ka < k_c a = (3/2)\phi \mathrm{Sc}^{-1}$. Numerical results reproduce quite exactly the theoretical trend for $F_c(k,t)$ at very small k but deviate as it is made larger. In terms of the relative difference $\Delta_k = (k_c - k)/k_c$, differences between the $k \to 0$ theoretical limit and simulations are 10% for $\Delta_k = 0.4$ to just 3% for $\Delta_k = 0.7$. The $k \to 0$ limit [25] neglects in-plane vorticity diffusion ($k^2\nu$) in favor of the transient advection ($\partial_t v \sim k^0$). As k is increased, below the crossover wave number $k < k_c$ we observe that diffusion of in-plane vorticity adds some contribution to $F_c(k,t)$.

The phenomenon of hydrodynamic enhancement of collective diffusion in confined media has been ascribed to *long-time* diffusion [10,14]. The systems hereby considered were not dense enough to exhibit the slowdown of diffusion at long times. However, we think that this statement needs to be revised. The physics of the long-time diffusion is probably not affected by hydrodynamics, being determined by steric and potential forces between elements in dense media. This long-time diffusion regime is preceded by a temporal window of anomalous diffusion, where memory arising from slowly varying global configurations alter the MSD exponent (it becomes smaller than one). The role of hydrodynamics in the anomalous diffusion of highly packed colloids or smaller molecules moving in confined systems is still to be explored.

To conclude, we mention an important open question which regards the role of walls in collective diffusion of colloids near or confined between walls. Colloids near walls is a ubiquitous problem in colloidal science whose dynamics can be now studied using evanescent wave dynamics [30]. Previous experimental works on colloids near a wall report an increase in $D_c(q)$ with decreasing q [31]. However, these results corresponds to the small-wave-number range $q\,a > 1$ where the increase in $D_c(q)$ arises from the osmotic pressure [i.e., from a reduction in $S(q)$] and not from hydrodynamics [see Fig. 5(a) for WCA]. In fact, the authors of Ref. [31] mention a reduction of D_c with respect the 3D case. Other experiments observed some increase in the diffusion of certain collective modes of a group of six close-by colloids [32] and suggest the relevance of three-body interactions (interestingly, at intermediate wave number, we also observe an increase in D_c due to three-body interactions). We are not aware of any work studying the analog of the hydrodynamic divergence of $D_c(q)$ in single-wall confinement. However, under two-wall confinement, recent experiments [11] report a study of $F_c(q,t)$ showing surprisingly large enhancements of collective diffusion. Colloids of about 1.5 microns in a slit of about 1.8–3.0 microns showed $D_c \sim 1/q^{\alpha}$ with $\alpha \in [1.7, 1.9]$. Such large exponents might be due to fluid slippage near the walls [11], although this is still an open question. The common source of the hydrodynamic enhancement of collective diffusion is the presence of a nonvanishing gradient (more properly, divergence) of the mutual mobility. Such a scenario is probably present near walls and in fact theoretical analysis on the mobility of two colloids indicate $\mathcal{M}_{12} \sim 1/r^2$, with r the distance between two colloids [33,34]. In view of these findings, the simulation of the hydrodynamic enhancement of diffusion close to near walls requires accurate models able to resolve the near-field hydrodynamics (up to 10% of the colloid radius) and three-body interactions. One candidate is the multiblob model for colloids [21,22] based on Eulerian-Lagrangian approaches. Stokesian dynamics is indeed another alternative; however, it is limited by the accuracy of the mobility kernels (see, e.g., Ref. [12]). Moreover, the scheme should allow us to model slip and no-slip surfaces and, ideally, partial slip.

ACKNOWLEDGMENTS

We thank Aleksandar Donev for a critical reading of the manuscript. We acknowledge the support of the Spanish Ministry of Science and Innovation MINECO (Spain) under Grant No. FIS2013-47350-C5-1-R and the "María de Maeztu" Programme for Units of Excellence in R&D (MDM-2014-0377). We also acknowledge the donors of The American Chemical Society Petroleum Research Fund for partial support of this research.

APPENDIX A: DERIVATION OF H_c

We start from expression (16) for the crossed hydrodynamic mobility, where we use a pairwise microscopic diffusion matrix $\mathbf{D}_{ij} = \mathbf{D}_{ij}(\mathbf{q}_{ij})$, such as the Oseen approximation in Eq. (15). This is,

$$H_c(k) = N \int P_2(\mathbf{q}_1,\mathbf{q}_2)\hat{\mathbf{k}} \cdot \frac{\mathbf{D}_{12}(\mathbf{q}_{12})}{D_0} \cdot \hat{\mathbf{k}} \times \exp[-i\mathbf{k}\cdot\mathbf{q}_{12}]d\mathbf{q}_1 d\mathbf{q}_2, \quad \text{(A1)}$$

where $P_2(\mathbf{q}_1,\mathbf{q}_2)$ is the reduced two-particle probability. It is convenient to work in the two-particle system's reference by introducing

$$\mathbf{R} = \frac{\mathbf{q}_2 + \mathbf{q}_1}{2}, \text{ and } \mathbf{r} = \mathbf{q}_2 - \mathbf{q}_1.$$

In these coordinates, the two-particle probability P_2 for dilute suspension becomes

$$P_2(\mathbf{R},\mathbf{r}) = \frac{1}{\mathcal{Z}_2}\exp\{-\beta[\Psi(\mathbf{r}) + V(Z,z)]\}. \quad \text{(A2)}$$

In the case of a confining harmonic potential it is possible to separate the action of the external potential into the center-of-mass $\mathbf{R}$ and the relative coordinate $\mathbf{r}$ as

$$\begin{aligned} V(Z,z) &= V_1(Z+z) + V_2(Z-z) \\ &= \frac{k_s}{2}\left[2Z^2 + \frac{1}{2}z^2\right] \equiv V_R(Z) + V_r(z). \end{aligned}$$

We use the notation V_R and V_r to alleviate expressions. This kind of separation is not generally applicable to any confining potential. For instance, for an exponential trap, $V(z) = \exp(-az)$, $V(Z+z) + V(Z-z) = 2\exp(-\alpha Z)\cosh(\alpha z)$.

In the following, in-plane coordinates will be denoted by "$\mathbf{s}$",

$$\mathbf{r} = \mathbf{s} + z\hat{\mathbf{z}}.$$

Considering the case of ideal colloids ($\Psi(\mathbf{r}) = 0$), one has

$$H_c(k) = B\int d^3r e^{-\beta V_r(z)}\hat{\mathbf{k}}\cdot\frac{\mathbf{D}_{12}(\mathbf{r})}{D_0}\cdot\hat{\mathbf{k}}\exp\{-i\mathbf{k}\cdot\mathbf{r}\}, \quad \text{(A3)}$$

where $\mathbf{k}$ is a two-dimensional vector over the confining plane, i.e., $\mathbf{k}\cdot\hat{\mathbf{z}} = 0$ and

$$B \equiv \frac{N\int d^3R e^{-\beta V_R(Z)}}{\mathcal{Z}_2} = \frac{N}{\int dr^3\exp[-\beta V_r(z)]} = \frac{\rho_{2D}\sqrt{\beta k_s}}{2\sqrt{\pi}}.$$

Introducing the inverse Fourier transform of $\mathbf{D}_{12}(\mathbf{r})$ with

$$\frac{\mathbf{D}_{12}(\mathbf{r})}{D_0} = \frac{1}{(2\pi)^3\mu_0}\int d^3\mathbf{k}' e^{i\mathbf{k}'\cdot\mathbf{r}}\frac{1}{\eta k'^2}\left[\mathbf{I} - \frac{\mathbf{k}'\mathbf{k}'}{k'^2}\right],$$

and substituting in Eq. (A3),

$$\begin{aligned} H_c(k) = \frac{B}{(2\pi)^3\mu_0}\int dz e^{-\beta k_s\frac{z^2}{4}}\hat{\mathbf{k}}\cdot\int d^3k'\frac{1}{\eta k'^2}\left[\mathbf{I} - \frac{\mathbf{k}'\mathbf{k}'}{k'^2}\right] \\ \times e^{ik'_z z}\cdot\hat{\mathbf{k}}\int d\mathbf{s} e^{-i\mathbf{k}\cdot\mathbf{s}}e^{i\mathbf{k}'_\parallel\cdot\mathbf{s}}. \end{aligned}$$

Writing $\hat{\mathbf{k}}\cdot\frac{\mathbf{D}_{12}(\mathbf{r})}{D_0}\cdot\hat{\mathbf{k}}\mu_0\eta = \frac{k'^2_\parallel + k'^2_z - (\hat{\mathbf{k}}\cdot\mathbf{k}')^2}{(k'^2_\parallel + k'^2_z)^2}$ and using $\int d\mathbf{s}\exp\{-i\mathbf{s}\cdot(\mathbf{k} - \mathbf{k}'_\parallel)\} = (2\pi)^2\hat{\delta}^2(\mathbf{k} - \mathbf{k}'_\parallel)$ (where $\hat{\delta}$ is the Dirac δ function) one thus obtains

$$H_c(k) = \frac{B}{(2\pi)\mu_0\eta}\int_{-\infty}^{\infty} dk'_z\frac{k'^2_z}{\left(k'^2_z + k^2\right)^2}\mathcal{V}(k'_z), \quad \text{(A4)}$$

where $\mathcal{V}(k'_z)$ is the 1D Fourier transform of the Boltzmann factor associated to the confining potential,

$$\mathcal{V}(k'_z) \equiv \int_{-\infty}^{\infty} dz e^{-\beta V_r(z)}e^{ik'_z z}.$$

Equation (A4) clearly indicates the effect of the soft confining potential. The strict 2D confinement corresponds to the limit to $P_2(R,r) \to \hat{\delta}(z)\hat{\delta}(Z)$ and $\mathcal{V}(k'_z) \to 1$, for which one recovers the expression derived in previous papers [10]. Under a softer confinement $\mathcal{V}(k'_z) = 2\sqrt{\pi}\delta\exp[-(k'_z\delta)^2]$ acts as a long-wave-number filter damping out contributions in the integral with $k'_z > \delta^{-1}$ such as

$$H_c(k) = \frac{B\delta}{\sqrt{\pi}\mu_0\eta}\int_{-\infty}^{\infty} dk'_z\frac{k'^2_z}{\left(k'^2_z + k^2\right)^2}e^{-(k'_z\delta)^2}. \quad \text{(A5)}$$

Integrating Eq. (A5) it yields

$$H_c(k) = 3\phi\frac{\delta}{a}\left\{\left[\frac{1}{2}(k\delta)^{-1} + (k\delta)\right]e^{(k\delta)^2}\mathrm{erfc}(k\delta) - \frac{1}{\sqrt{\pi}}\right\}. \quad \text{(A6)}$$

APPENDIX B: NUMERICAL METHODS

1. Colloidal hydrodynamics with FLUAM

Numerical simulations of the dynamics of a colloid assembly under confinement have been performed using our immersed boundary hydrodynamic solver, FLUAM (acronym for *FLuid And Matter*). FLUAM is a free open-source code running in GPU [15]. The fluid phase is solved using a finite volume solver for incompressible fluctuating hydrodynamics [35] and it is equipped with the immersed boundary method to couple fluid and particle dynamics. We consider neutrally buoyant particles (i.e., without inertia) in and incompressible fluid. Although colloid dynamics usually correspond to the Stokes limit, where the fluid momentum has negligible inertia, we kept the transient term in the fluid momentum equation to investigate the non-over-damped regime of collective diffusion, in Sec. V. The equations solved by FLUAM are

$$\rho_f\partial_t\mathbf{v} = -\nabla p + \eta\nabla^2\mathbf{v} + \sum_i \mathbf{F}_i S(\mathbf{r} - \mathbf{q}_i), \quad \text{(B1)}$$

$$\nabla\cdot\mathbf{v} = 0, \quad \text{(B2)}$$

$$\dot{\mathbf{q}}_i \equiv \mathbf{u}_i = \int d\mathbf{r} S(\mathbf{r} - \mathbf{q}_i)\mathbf{v}(\mathbf{r}). \quad \text{(B3)}$$

Here $\rho_f = 1$ is the constant fluid density (used as reference), $\mathbf{v}(\mathbf{r})$ is the fluid velocity field, $\mathbf{F}_i$ is the total force acting on particle "i," and p is the mechanic pressure which guarantees incompressibility $\nabla\cdot\mathbf{v} = 0$. The third kinetic condition guarantees that the particle velocity $\mathbf{u} = d\mathbf{q}/dt$ equals the velocity of the fluid it displaces, as it should be. Note that $\mathbf{q}_i(t)$ is the position vector of particle "i" while $\mathbf{r}$ denotes the Eulerian (fixed) coordinates of the fluid. In practice, Eq. (B1) is spatially discretized in a regular-grid of size h, containing M_α fluid cells per direction α. The grid size is our reference length $h = M_\alpha/L_\alpha = 1$. The time evolution of the fluid and particle equations is discretized with a time step Δt, whose maximum value is determined by the fastest process, according to the Courant stability condition. Here $\Delta t < h^2/\nu$.

In Eq. (B1) the force acting on each colloid $\mathbf{F}_i$ is locally transferred, or spread, to the fluid as a force density. The spreading operation is carried out using a kernel of compact support which moves concomitant to (each) particle position, $S(\mathbf{r} - \mathbf{q}_i)$. In this minimal resolution model, each kernel corresponds to a single "colloid" or to a "blob," which is the term we used in previous papers. The kernel, which has units of inverse volume, acts like a regularized Dirac δ. But, contrary to the Dirac δ used to represent a point-particle disturbance, this kernel provides a finite hydrodynamic radius R_h to the blob.

TABLE I. Parameters used in hydrodynamic simulations (FLUAM).

Parameter	Description	Value
h	Cell dimension	1
k_bT	Thermal energy	1
ρ_f	Fluid density	1
μ	Fluid viscosity	[0.5–7]
m_e	Colloid excess mass	0
R_h	Hydrodynamic radius	$0.91h$
σ	Colloid LJ diameter	$2h$
a	Nominal radius: ideal colloids	R_h
a	Nominal radius: nonideal colloids	$\sigma/2$
ϵ	Colloid LJ energy	$1.36k_bT$
Δt	Time step	0.1
τ_{GPU}/τ	GPU time/step	3.8 ms

Here we use a 3-point Peskin kernel for which $R_h = 0.91\,h$. It also provides a mutual mobility tensor compatible with level of resolution of the Rotne-Prager-Yamawaka model. For an unabridged description, we refer to Refs. [23,36] and references therein.

Simulations were typically performed in rectangular periodic boxes of sides $L_x \times L_y \times L_z = (64 \times 64 \times 16)h^3$. Calculations with increased length in z direction were also performed to check for any finite-size effects on the shorter confining direction z. Interestingly, the finite box effects we faced were revealed by discrepancies with the theoretical solutions at hand. In particular, for the softest confinements we had to work with boxes of sides $128 \times 128 \times 100\,h^3$ to avoid interference from the periodic images of the colloid sheet.

a. Systems studied

We studied three types of colloidal systems, ideal colloids (ideal particles) and short ranged potentials: the purely repulsive WCA and the Lennard-Jones potential with cutoff 2.5σ, where the diameter of the interparticle potential is $\sigma = 2\,h$, and the size of the fluid grid h is taken as a reference length. The potential interaction energy was set to $\epsilon = 1.36k_BT$. Details of the simulation parameters are given in Table I.

b. Schmidt number

The bare diffusion of one particle is given by the Stokes-Einstein formula $D_0 = k_BT/(6\pi\eta R_h)$. The Schmidt number, the ratio between the fluid momentum diffusion and the bare mass diffusion coefficient, $\mathrm{Sc} = \nu/D_0$ (with $\nu = \eta/\rho_f$ the kinematic viscosity), is extremely large for any colloid suspended in a liquid. As shown in Ref. [24], to safely recover the Stokes limit regime one requires $\mathrm{Sc} > 100$. The Stokes-Einstein-based Schmidt number $\mathrm{Sc} = 6\pi\eta^2 R_h/(\rho_f k_B T)$ can be controlled by increasing the fluid kinematic viscosity. Results in Sec III A and IV, corresponding to the Stokes limit regime, were carried out for $\mathrm{Sc} \simeq 900$.

Surface density $\rho_{2D} = N/A$ and area $A = L_xL_y$ was varied in the range $\phi = 0.03$ to 0.54. The largest value corresponds to an average interparticle distance of $\rho_{2D}^{-1/2} = 2.65R_h$, which is a reasonable limit for the accuracy of the blob model in term of mutual mobility [36].

c. Confining potential

The confining potential was varied in the range $k_s \in [0.1,50]$ corresponding to a range of confinement width $\delta \in [0.14,3.16]\,h$ (recall $k_BT = 1$ is used as reference, see Table I). For the softest confinement, with $\delta = 3.16h$, we had to increase the length of the box in z direction to avoid hydrodynamic coupling between periodic images of the system. We tried $L_z = 32\,h$ and $64\,h$, observing convergence on $L_z = 32h$ (which is about 10 times δ).

2. Brownian dynamics without HI

Simulations without hydrodynamic interactions were performed with the GROMACS package [37,38]. The solver performs the standard BD,

$$d\mathbf{q}_i = \mu_0\mathbf{F}_i dt + (2k_B\mu_0)^{1/2} d\mathbf{W}_i, \tag{B4}$$

where $\mathbf{F}_i$ is the total force applied on the ith molecule, μ_0 the bare mobility, and the white (time uncorrelated) noise covariance is

$$\langle d\mathbf{W}_i(t) d\mathbf{W}_j(t)\rangle = \delta_{ij} dt \tag{B5}$$

[1] C. P. Kelleher, A. Wang, G. I. Guerrero-García, A. D. Hollingsworth, R. E. Guerra, B. J. Krishnatreya, D. G. Grier, V. N. Manoharan, and P. M. Chaikin, Phys. Rev. E **92**, 062306 (2015).

[2] A. Domínguez, M. Oettel, and S. Dietrich, Phys. Rev. E **82**, 011402 (2010).

[3] P. Gao, Z. Yi, X. Xing, T. Ngai, and F. Jin, Langmuir **32**, 4909 (2016).

[4] G. Whitworth and W. T. Coakley, J. Acoust. Soc. Am. **91**, 79 (1992).

[5] H. Bruus, J. Dual, J. Hawkes, M. Hill, T. Laurell, J. Nilsson, S. Radel, S. Sadhal, and M. Wiklund, Lab on a Chip **11**, 3579 (2011).

[6] M. Settnes and H. Bruus, Phys. Rev. E **85**, 016327 (2012).

[7] F. Balboa Usabiaga and R. Delgado-Buscalioni, Phys. Rev. E **88**, 063304 (2013).

[8] X. Ding, J. Shi, S.-C. S. Lin, S. Yazdi, B. Kiraly, and T. J. Huang, Lab on a chip **12**, 2491 (2012).

[9] K. Zahn, R. Lenke, and G. Maret, Phys. Rev. Lett. **82**, 2721 (1999).

[10] J. Bleibel, A. Domnguez, and M. Oettel, J. Phys.: Condens. Matter **27**, 194113 (2015).

[11] B. Lin, B. Cui, X. Xu, R. Zangi, H. Diamant, and S. A. Rice, Phys. Rev. E **89**, 022303 (2014).

[12] R. Pesché and G. Nägele, Phys. Rev. E **62**, 5432 (2000).

[13] J. Bleibel, A. Domnguez, and M. Oettel, J. Phys.: Condens. Matter **28**, 244021 (2016).

[14] A. Domínguez, Phys. Rev. E **90**, 062314 (2014).

[15] F. Balboa Usabiaga, FLUAM, https://github.com/fbusabiaga/fluam.

[16] J. Bleibel, A. Dominguez, F. Gunther, J. Harting, and M. Oettel, Soft Matter **10**, 2945 (2014), URL http://dx.doi.org/10.1039/C3SM53043D.

[17] J. Dhont, *An Introduction to Dynamic of Colloids* (Elsevier, Amsterdam, 1996), Vol. 2.
[18] C. L. Armstrong, Ph.D. thesis, McMaster University, McMaster University, Hamilton, Ontario, 2013.
[19] D. J. Mller, A. Engel, U. Matthey, T. Meier, P. Dimroth, and K. Suda, J. Mol. Biol. **327**, 925 (2003).
[20] P. Hopkins, A. Fortini, A. J. Archer, and M. Schmidt, J. Chem. Phys. **133**, 224505 (2010).
[21] F. B. Usabiaga, B. Kallemov, B. Delmotte, A. Bhalla, B. E. Griffith, and A. Donev, arXiv:1602.02170 (2016).
[22] A. Vazquez-Quesada, F. B. Usabiaga, and R. Delgado-Buscalioni, J. Chem. Phys. **141**, 204102 (2014).
[23] F. B. Usabiaga, I. Pagonabarraga, and R. Delgado-Buscalioni, J. Comput. Phys. **235**, 701 (2013).
[24] F. Balboa Usabiaga, X. Xie, R. Delgado-Buscalioni, and A. Donev, J. Chem. Phys. **139**, 214113 (2013).
[25] M. Oettel, A. Domínguez, and S. Dietrich, Phys. Rev. E **71**, 051401 (2005).
[26] B. Lin, S. A. Rice, and D. A. Weitz, Phys. Rev. E **51**, 423 (1995).
[27] T. Apajalahti, P. Niemela, P. N. Govindan, M. S. Miettinen, E. Salonen, S.-J. Marrink, and I. Vattulainen, Faraday Discuss. **144**, 411 (2010).
[28] C. Brangwynne, G. Koenderink, F. C. MacKintosh, and D. A. Weitz, J. Cell Biol. **183**, 583 (2008).
[29] T. Gurin, J. Prost, P. Martin, and J.-F. Joanny, Current Opinion in Cell Biology **22**, 14 (2010).
[30] J. W. Swan and J. F. Brady, J. Chem. Phys. **135**, 014701 (2011).
[31] V. N. Michailidou, J. W. Swan, J. F. Brady, and G. Petekidis, J. Chem. Phys. **139**, 164905 (2013).
[32] P. P. Lele, J. W. Swan, J. F. Brady, N. J. Wagner, and E. M. Furst, Soft Matter **7**, 6844 (2011).
[33] E. R. Dufresne, T. M. Squires, M. P. Brenner, and D. G. Grier, Phys. Rev. Lett. **85**, 3317 (2000).
[34] H. Diamant, B. Cui, B. Lin, and S. A. Rice, J. Phys.: Condens. Matter **17**, S2787 (2005).
[35] F. B. Usabiaga, J. B. Bell, R. Delgado-Buscalioni, A. Donev, T. G. F. Boyce, E. Griffith, and C. S. Peskin, Multiscale Model. Simul. **10**, 1369 (2012).
[36] F. B. Usabiaga, R. Delgado-Buscalioni, B. E. Griffith, and A. Donev, Comput. Methods Appl. Mech. Eng. **269**, 139 (2014).
[37] D. Van Der Spoel, E. Lindahl, B. Hess, G. Groenhof, A. E. Mark, and H. J. C. Berendsen, J. Comput. Chem. **26**, 1701 (2005).
[38] B. Hess, C. Kutzner, D. Van Der Spoel, and E. Lindahl, J. Chem. Theory Comput. **4**, 435 (2008).